Supplementary Information

Synergistic Optimization of Carrier Transport and Thermal Conductivity in Sn-doped Cu_2Te

Yuchong Qiu, Ying Liu, Jinwen Ye, Jun Li, Lixian Lian*

College of Materials Science and Engineering, Sichuan University, Chengdu 610065, P. R. China

Corresponding author: liuying5536@scu.edu.cn

In a single parabolic band (SPB) model, the relationships between different physical parameters can be expressed as:[1-3]

Seebeck coefficient:

$$S = \pm\frac{k_B}{e}\left(\frac{(r+5/2)F_{r+3/2}(\eta)}{(r+3/2)F_{r+1/2}(\eta)} - \eta\right) \quad \text{Equation (S1)}$$

Carrier concentration:

$$n_H = \frac{(2m^* k_B T)^{3/2}}{h^3 2\pi^2}\frac{F_{1/2}(\eta)}{r_H} \quad \text{Equation (S2)}$$

Hall factor:

$$r_H = \frac{3}{4}\frac{F_{1/2}(\eta)F_{-1/2}(\eta)}{F_0^2(\eta)} \quad \text{Equation (S3)}$$

Carrier mobility:

$$\mu_H = \mu_0\frac{\sqrt{\pi}}{2}\frac{F_0(\eta)}{F_{1/2}(\eta)} \quad \text{Equation (S4)}$$

Electrical conductivity:

$$\sigma = n_{\mathrm{H}} \mu_{\mathrm{H}} e$$ Equation (S5)

Fermi integral:

$$F_n(\eta) = \int_0^{\infty} \frac{\chi^n}{\exp(\chi - \eta) + 1} \mathrm{d}\chi$$ Equation (S6)

Reduced Fermi energy:

$$\eta = \frac{E_{\mathrm{F}}}{k_{\mathrm{B}} T}$$ Equation (S7)

Lorentz number:

$$L = \left(\frac{k_B}{e} \right)^2 \left(\frac{(r + 7/2) F_{r+5/2}(\eta)}{(r + 3/2) F_{r+1/2}(\eta)} - \left[\frac{(r + 5/2) F_{r+3/2}(\eta)}{(r + 3/2) F_{r+1/2}(\eta)} \right]^2 \right)$$ Equation (S8)

In the above equations, k_{B} is the Boltzmann constant, e is the elementary charge, r is the scattering factor, η is the reduced Fermi energy, m^* is the density-of-states effective mass, χ is the reduced carrier energy.

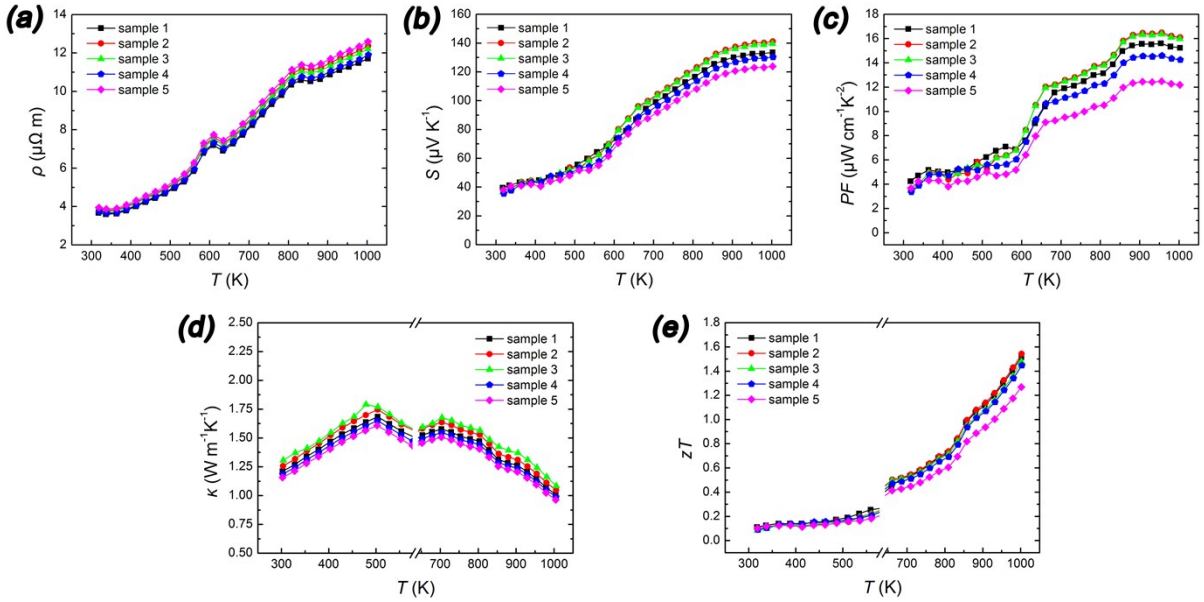

Figure S1. Temperature-dependent thermoelectric properties for 5 independent samples ($Cu_{1.90}Sn_{0.10}Te$). (a) electrical resistivity, ρ; (b) Seebeck coefficient, S; (c) power factor, $S^2\sigma$; (d) thermal conductivity, κ; (e) zTs.

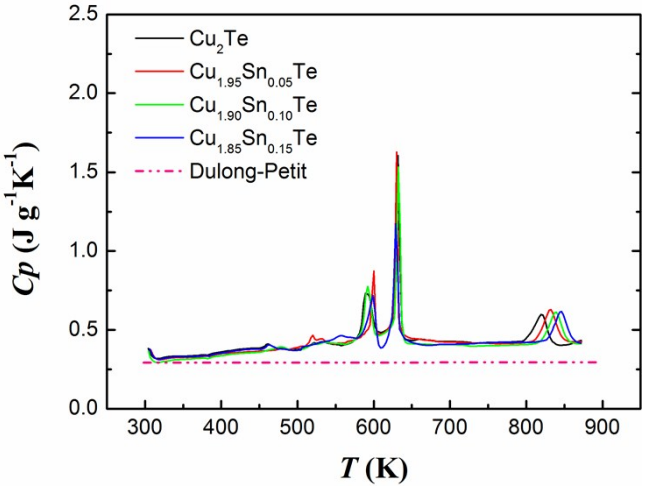

Figure S2. Temperature-dependent C_p for different compositions.

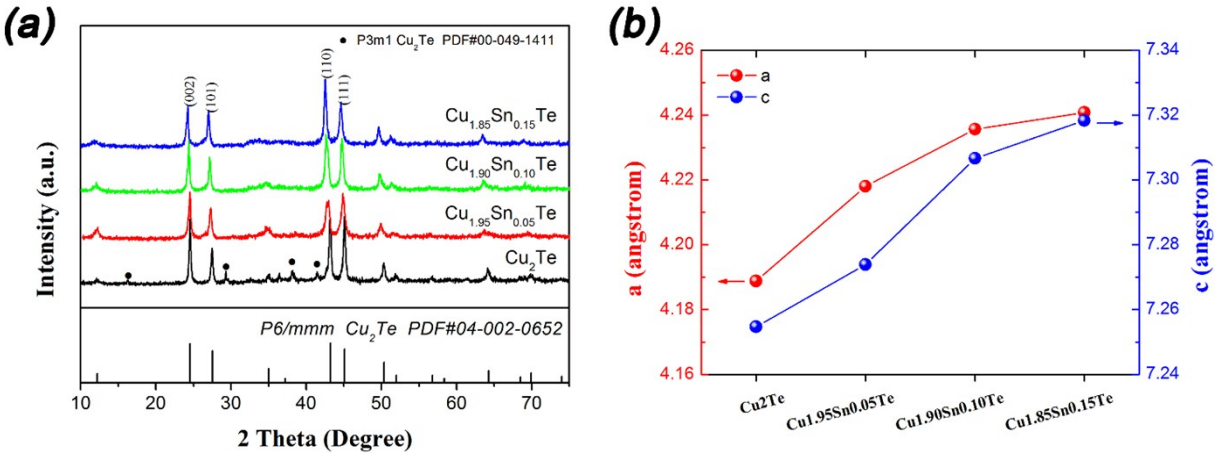

Figure S3. (a) XRD patterns for $Cu_{1-x}Sn_xTe$. (b) Variation of lattice constant *a* and *c* with Sn content.

XRD results show that all the sintered samples could be indexed to the hexagonal Cu_2Te (P6/mmm, PDF#04-002-0652) and no detectable impurities, such as SnTe, were found with the introduction of Sn. Both the lattice constant *a* and *c* increased with rising content of Sn, implying lattice expansion caused by either the filling of Cu vacancies by Sn atoms or the replacement for Cu atoms by the relative larger Sn atoms.

Two structures (P6/mmm and P3m1) exist in pristine Cu_2Te. While only the primary P6/mmm structure exists in Sn containing samples, indicating that the incorporation of Sn might also purify Cu_2Te phase.

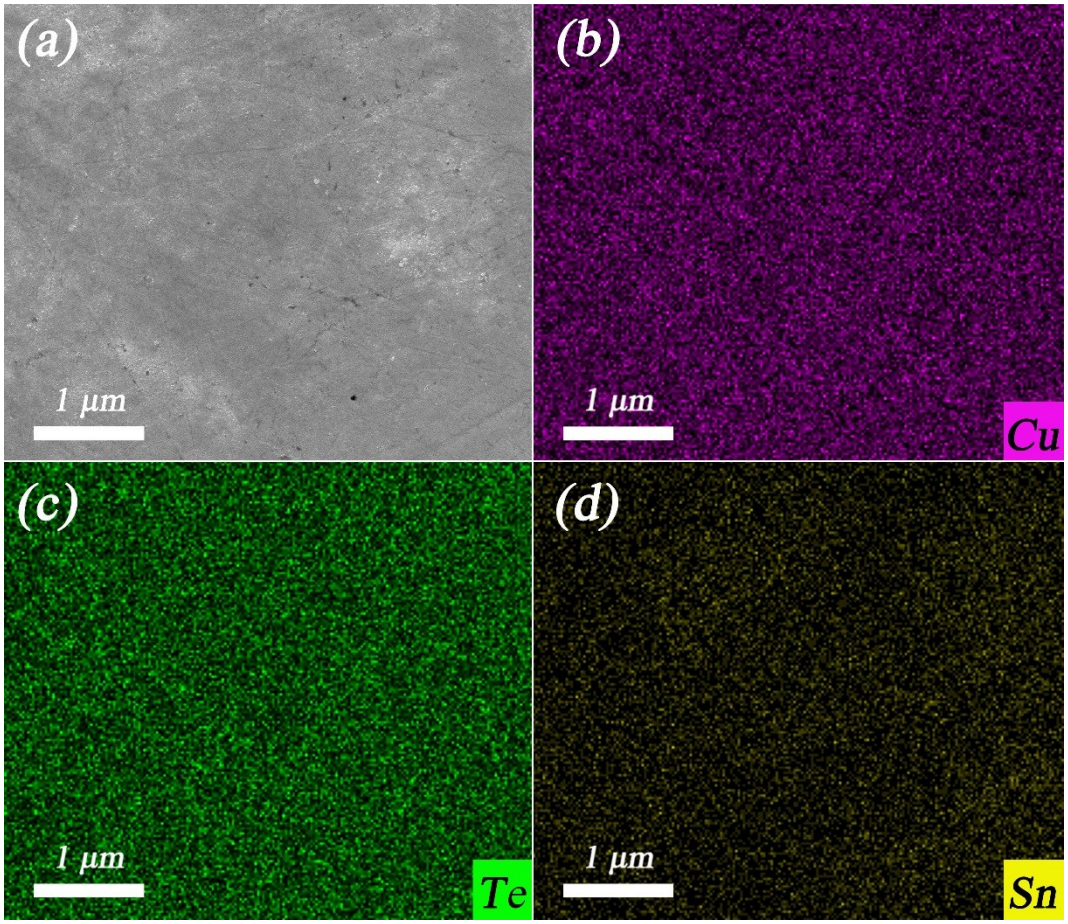

Figure S4. (a) SEM image of $Cu_{1.90}Sn_{0.10}Te$ polished sample; (b) elemental mapping for Cu; (c) elemental mapping for Te; (d) elemental mapping for Sn.

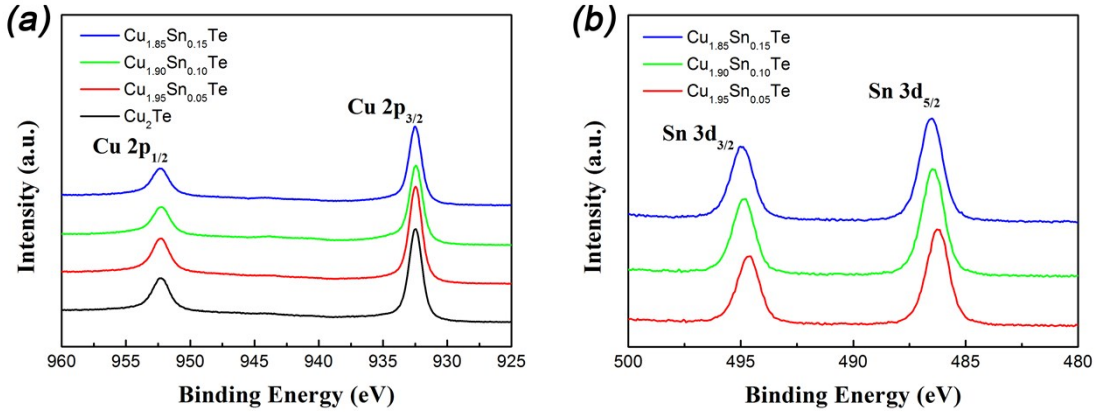

Figure S5. XPS core level spectra for different compositions. (a) Cu $2p_{1/2}$ and $2p_{3/2}$ excitation peak; (b) Sn $3d_{3/2}$ and $3d_{5/2}$ excitation peak.

Table S1. Chemical compositions determined by ICP and the calculated stoichiometry.

Designed composition	Cu_2Te	$Cu_{1.95}Sn_{0.05}Te$	$Cu_{1.90}Sn_{0.10}Te$	$Cu_{1.85}Sn_{0.15}Te$
Cu (wt.%)	49.15	48.37	47.20	44.15
Te (wt.%)	50.85	49.51	48.69	50.10
Sn (wt.%)	\	2.12	4.11	5.75
Formula calculated from the measured contents	$Cu_{1.97}Te_{1.01}$	$Cu_{1.96}Sn_{0.05}Te_{1.00}$	$Cu_{1.93}Sn_{0.09}Te_{0.99}$	$Cu_{1.83}Sn_{0.13}Te_{1.03}$

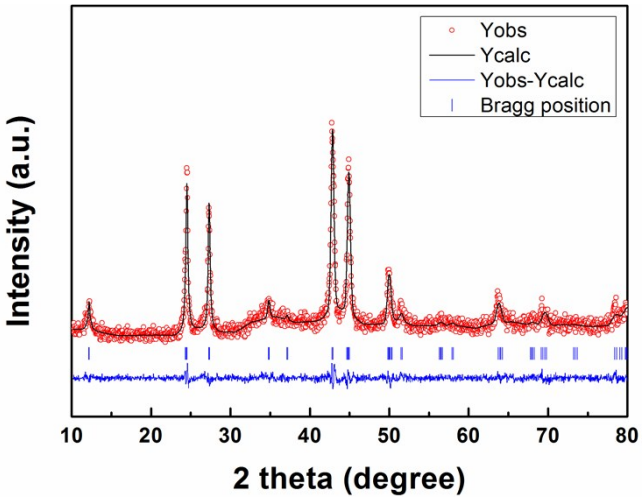

Figure S6. XRD refinement of $Cu_{1.90}Sn_{0.10}Te$.

Table S2. Crystallographic information obtained by XRD refinement for $Cu_{1.90}Sn_{0.10}Te$

Space group	a	b	c	α	β	γ
P/6mmm	4.22106 Å	4.22106 Å	7.26098 Å	90°	90°	120°

Table S2. Crystallographic information obtained by XRD refinement for $Cu_{1.90}Sn_{0.10}Te$

	Wyckoff site	x	y	z	B	Occ
Cu	4h	0.33333	0.66667	0.22908	0.42218	0.93033
Sn	4h	0.33333	0.66667	0.32442	0.06292	0.05546
Te	2e	0	0	0.17364	0.09825	0.98281
R_{wp}	2.9826	R_{exp}	1.7300	χ^2	2.9723	

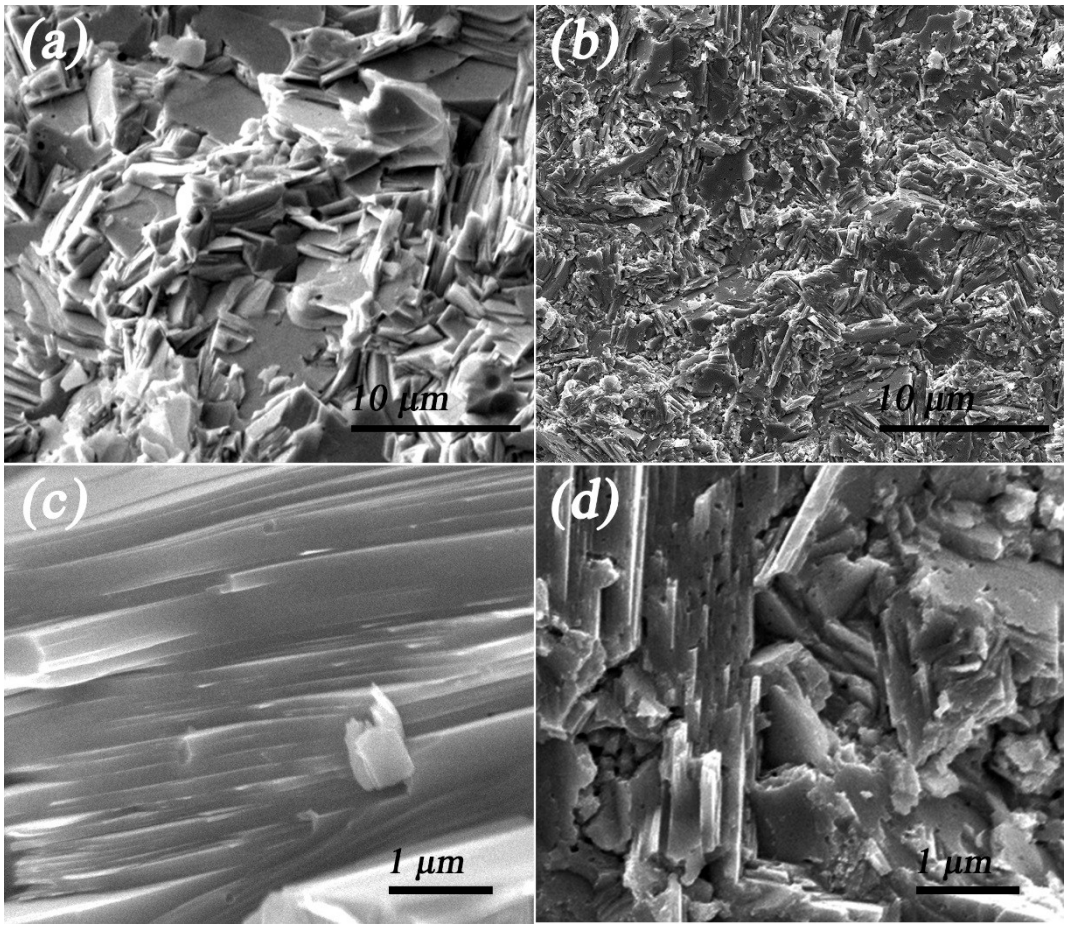

Figure S7. SEM images of fracture surface. (a) Cu_2Te; (b) $Cu_{1.90}Sn_{0.10}Te$; (c) high magnification focused in the layered structure for Cu_2Te; (d) high magnification focused in the layered structure for $Cu_{1.90}Sn_{0.10}Te$.

SEM investigations show that doping Sn could efficiently decrease the grain size of Cu_2Te. While the layer thickness is not obviously affected.

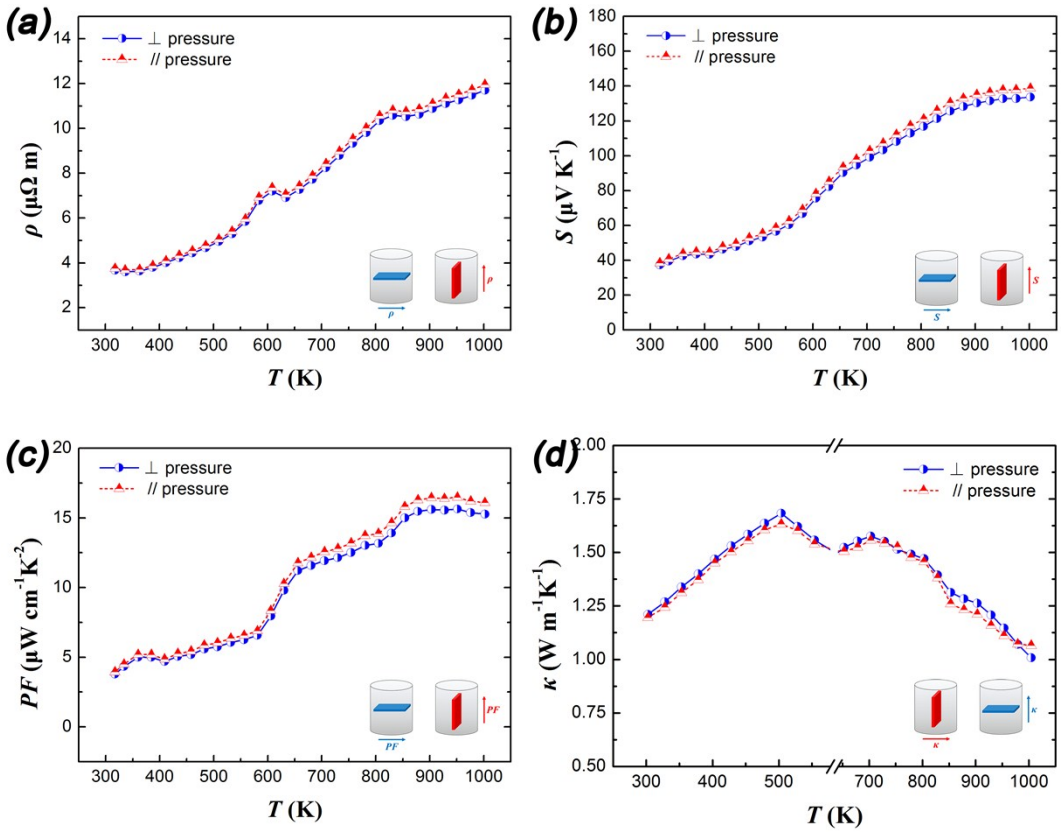

Figure S8. Temperature-dependent thermoelectric properties for $Cu_{1.90}Sn_{0.10}Te$ parallel and vertical to pressure direction. (a) electrical resistivity, ρ; (b) Seebeck coefficient, S; (c) power factor, $S^2\sigma$; (d) thermal conductivity, κ.

Table S3. Phase transitions of Cu_2Te with according temperature.[4]

Phase transition	α-β	β-γ	γ-δ	δ-ε
Structure change	hex-hex	hex-ortho	ortho-hex	hex-cub
Temperature	~450 K	~600 K	~630 K	~760 to 850 K

Note: According to different preparation methods, the transition temperature might be altered within some temperature range. Especially, the last transition might span nearly a hundred kelvin due to composition difference. More details could refer to Vouroutzis's work.[5]

Table S4. Density of states effective mass for different composition at 300 K

Composition	Cu_2Te	$Cu_{1.95}Sn_{0.05}Te$	$Cu_{1.90}Sn_{0.10}Te$	$Cu_{1.85}Sn_{0.15}Te$
m_d* (unit m_e)	1.50	2.57	2.56	2.57

Owing to the ultrahigh n_H and multiple phase transitions for this material, it is difficult to separate the different portion contributed from electronic and lattice part from the total κ. In He's work,[6] the authors firstly assumed the lattice κ (κ_L) for Cu_2Te would be around 0.2 W $m^{-1}K^{-1}$, from which then they calculated the Lorentz number (L) to be 1.0-1.6×10^{-8} V^2K^{-2} in the T range of 700-800 K and 900-1000 K. From a technical point of view, we consider this method is not rigorous and not precise enough. And in Ballikaya's work,[7] the authors deemed that the very high electrical conductivity of the copper telluride might comprise contributions from both charge carriers and mobile Cu^+ ions, thus the determination of the κ_L would be difficult for the uncertainty of the Wiedemann-Franz law. Additionally, some previous studies revealed that sometimes Wiedemann-Franz law would be violated,[8-10] thus leading to unreal values of L.

Here in this work, we first carried out L calculations from the reduced Fermi energy (η) according to Equation S8 and obtained considerably large L value, ~2.42×10^{-8} V^2K^{-2} at RT and ~1.95×10^{-8} V^2K^{-2} at 1000 K. These large L values resulted in very high electronic κ (κ_e) that quite close to the total κ, making the κ_L unrealistically small or even negative at some T. Therefore, we consider that Wiedemann-Franz law should not be used in the κ_L estimation in copper telluride system, not only because it would probably overestimate the κ_e for these cation liquid-like compounds (migrating cations may also contribute to the electrical conductivity), but also because the scattering mechanism is quite complex during phase transitions where phonon-phonon might not dominate the carrier scattering.

Keyes relation has been often used to predict the κ_L of materials and proved to be solid in many cases.[1] Here in this paper, we absorbed the Keyes relation (Equation S9) to estimate the κ_L of all the samples based on the presupposition that the introduced dopant and phase transition would not cause any variation in κ_L. Of course, this presupposition is untenable, nevertheless here it just provides the general trends of κ_L with varying T for Cu_2Te-based "ideal crystals". κ_L as a function of T for the four samples are plotted below (Figure S9), in which it could be seen that the κ_L for all samples share a similar trend with rising T, roughly following $\sim T^{-1}$ rule.

Keyes relation:[1]

$$\kappa_L = \frac{B_K}{T}\frac{T_m^{3/2}\rho_d^{2/3}}{A^{7/6}} \qquad \text{Equation (S9)}$$

where B_K is the Keyes parameter, T_m is the melting temperature,[11] ρ_d is the density, A is the average atomic weight.

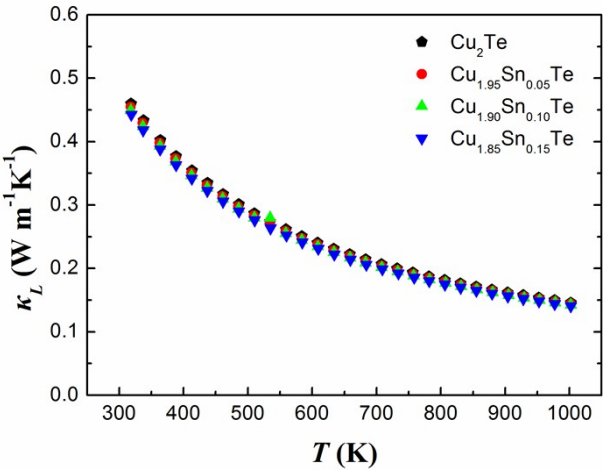

Figure S9. Lattice thermal conductivity (κL) calculated using the Keyes relation.

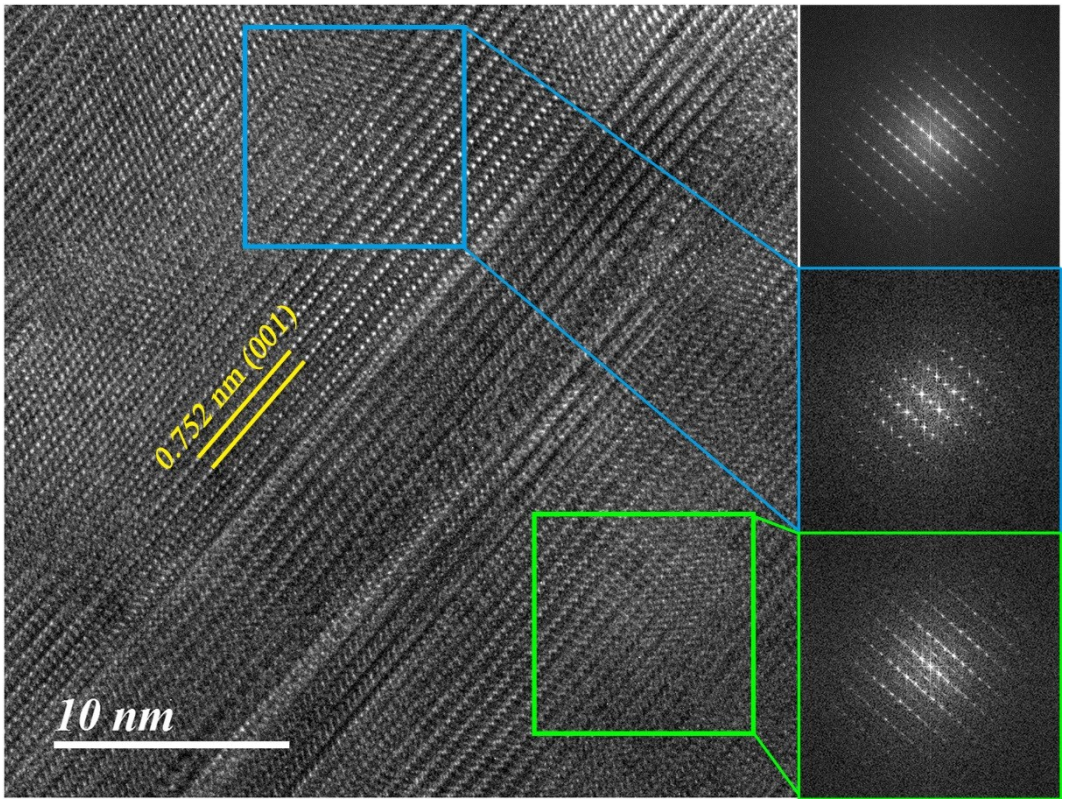

Figure S10. HRTEM of $Cu_{1.90}Sn_{0.10}Te$ showing different layer divided by slightly twisted boundary with corresponding FFT. The whole image FFT is shown in the upper right corner, the blue and green edged FFT in in the middle and bottom right side correspond to the blue and green squares in the HRTEM image.

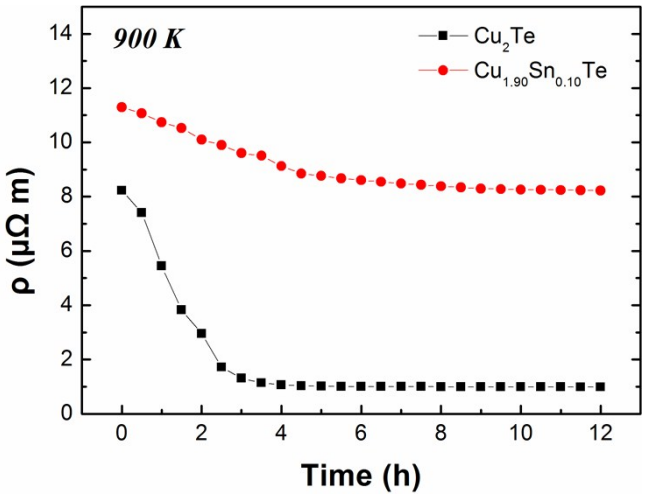

Figure S11. Electrical resistivity (ρ) for Cu_2Te and $Cu_{1.90}Sn_{0.10}Te$ measured at 900 K every 0.5 h for 12 h.

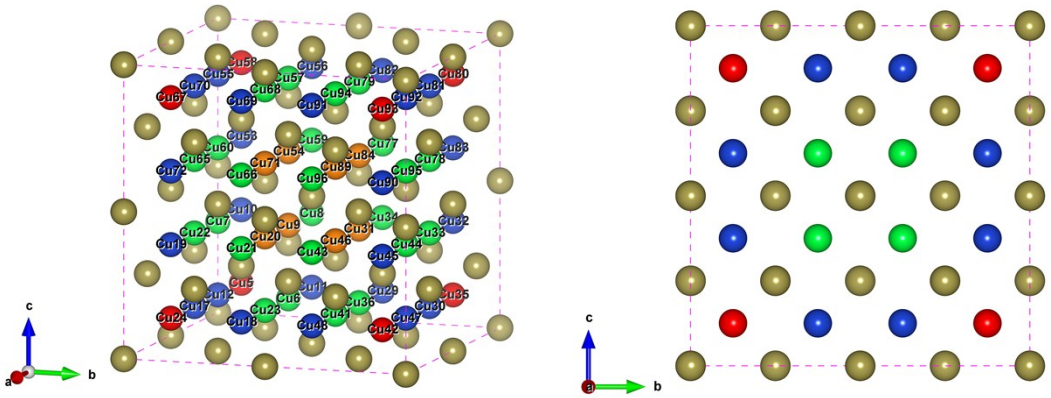

Figure S12. 2×2×2 supercell containing 64 Cu atoms and 32 Te atoms. There are 4 categories of Cu sites in the supercell denote as orange, green, blue, and red. Te atoms are marked as brown.

We simply treat the same color Cu sites as equivalent sites. And when vacancies or Sn atoms were introduced into the system, we avoided to put them in the neighboring equivalent sites. Thus, 8 possible substitutions were subjected to self-consistent geometry relaxation to check the lowest total energy. The results are shown below in Table S5. The results indicate that Substitution 5 could give the lowest total energy among all the calculated possibilities, therefore this substitution scheme was used for the following DOS and band structure calculations. Also, this substitution scheme was used in the Sn-doped structure.

Table S5. Total energy of possible substitutions for Cu_2Te supercell.

	Vacancy 1	**Vacancy 2**	**Vacancy 3**	**Total energy (eV)**
1	site 54 (orange)	site 43 (green)	site 88 (blue)	-337.396025529
2	site 54 (orange)	site 43 (green)	site 80 (red)	-337.555469100
3	site 54 (orange)	site 45 (blue)	site 80 (red)	-337.465225713
4	site 54 (orange)	site 23 (green)	site 78 (green)	-340.535436108
5	site 54 (orange)	site 22 (green)	site 78 (green)	-341.009657151
6	site 54 (orange)	site 18 (blue)	site 82 (blue)	-337.116928251
7	site 54 (orange)	site 24 (red)	site 80 (red)	-337.111689747
8	site 66 (green)	site 32 (blue)	site 58 (red)	-334.223971485

References:

1. H. J. Goldsmid, *Introduction to Thermoelectricity*, Springer, 2nd edn., 2016.
2. C. L. Chen, H. Wang, Y. Y. Chen, T. Day and G. J. Snyder, *J. Mater. Chem. A*, 2014, **2**, 11171-11176.
3. K. Zhao, A. B. Blichfeld, H. Chen, Q. Song, T. Zhang, C. Zhu, D. Ren, R. Hanus, P. Qiu, B. B. Iversen, F. Xu, G. J. Snyder, X. Shi and L. Chen, *Chem. Mater.*, 2017, **29**, 6367-6377.
4. Y. Qiu, J. Ye, Y. Liu and X. Yang, *RSC Adv.*, 2017, **7**, 22558-22566.
5. N. Vouroutzis and C. Manolikas, *Phys. Status Solidi A*, 1989, **111**, 491-497.
6. Y. He, T. Zhang, X. Shi, S.-H. Wei and L. Chen, *NPG Asia Mater.*, 2015, **7**, e210.
7. S. Ballikaya, H. Chi, J. R. Salvador and C. Uher, *J. Mater. Chem. A*, 2013, **1**, 12478-12484.
8. A. J. Minnich, M. S. Dresselhaus, Z. F. Ren and G. Chen, *Energ. Environ. Sci.*, 2009, **2**, 466-479.
9. N. Wakeham, A. F. Bangura, X. Xu, J.-F. Mercure, M. Greenblatt and N. E. Hussey, *Nat. Commun.*, 2011, **2**, 396.
10. S. Lee, K. Hippalgaonkar, F. Yang, J. Hong, C. Ko, J. Suh, K. Liu, K. Wang, J. J. Urban and X. Zhang, *Science*, 2017, **355**, 371-374.
11. R. Blachnik, M. Lasocka and U. Walbrecht, *J. Solid State Chem.*, 1983, **48**, 431-438.